Volume 12
Number 40
28 October 2024
Pages 16241–16632

Journal of Materials Chemistry C

Materials for optical, magnetic and electronic devices

rsc.li/materials-c

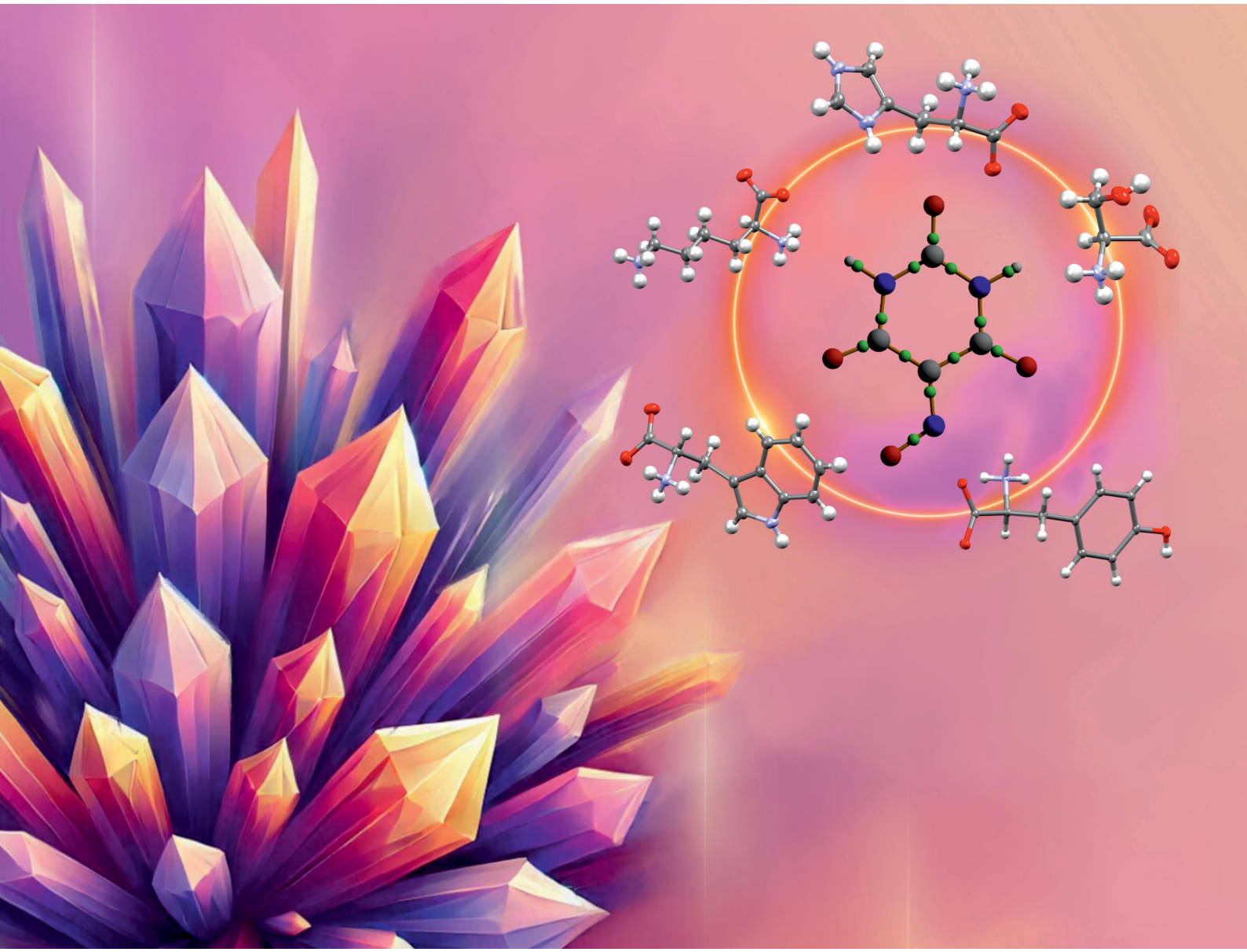

ISSN 2050-7526

ROYAL SOCIETY OF CHEMISTRY

PAPER

Marlena Gryl *et al.*

Deciphering colour mechanisms in co-crystals and salts containing violuric acid and chosen L-amino acids

Journal of Materials Chemistry C

ROYAL SOCIETY OF CHEMISTRY

PAPER

View Article Online
View Journal | View Issue

Cite this: J. Mater. Chem. C, 2024, 12, 16322

Deciphering colour mechanisms in co-crystals and salts containing violuric acid and chosen L-amino acids†

Agnieszka Rydz, Marlena Gryl, * Katarzyna Ostrowska and Katarzyna Marta Stadnicka

Received 26th July 2024,
Accepted 13th August 2024

DOI: 10.1039/d4tc03209h

rsc.li/materials-c

The understanding of colour origins in single-component materials is well established, however comprehending the factors that influence colour in multi-component crystalline phases remains a complex endeavor. This study addresses the challenge of predicting absorption properties in solid-state materials, crucial for designing systems for specific applications. We focused on six multi-component crystals based on violuric acid (VA) and selected L-amino acids, chosen for their chemical and structural diversity. This approach allowed us to explore various factors affecting absorption properties, including co-crystal and salt formation, hydrogen bonding, π–π interactions, amino acid side chain conformations, and solvent inclusion. Techniques such as X-ray diffraction, ^{1}H NMR spectroscopy, and UV-Vis spectroscopy were employed for detailed analysis of the structure and optical properties of the studied systems. The intermolecular interactions were scrutinized through the topology of electron density, Hirshfeld surface analysis, and the non-covalent interaction (NCI) index. UV-Vis titrations of crystallization solutions were also conducted to determine the binding constants of salts. This comprehensive study aims to enhance our understanding of absorption properties in multi-component materials.

Introduction

Colour chemistry attracts much attention because of the widespread applications of chromic materials as sensors,[1–3] molecular optical devices,[4,5] thermochromic inks[6,7] or dyes.[8] Chromic effects arise from the absorption or emission processes in a material due to applied external stimuli which can be, *e.g.* light, temperature, pressure, electric field or the presence of another substance.[7] Light absorption processes in the solid state seem to be well understood in many single-component systems, in which molecule under the influence of external stimulus undergoes, *e.g.*, *cis*/*trans* conformational transformation,[9] keto–enol tautomerism,[10,11] cyclization reactions,[12] or exhibit changes in the geometry of intermolecular interactions.[13,14] However, inducing absorption or emission at a precisely selected wavelength using specified chemical compounds remains a formidable challenge. Engineering such properties necessitates a profound understanding of molecular aggregation processes, which lead to distinct molecular arrangements found in the solid state.

Moreover, many acknowledged chromogens and chromophores may not be environmentally benign and sometimes are even considered toxic. Familiar instances include carcinogenic azo compounds[15] and the notorious pollution from textile dyes.[16] These cases pose substantial challenges to industrial applications. Finding new colorants, less harmful, is of crucial importance to the textile industry, environmental sustainability, and public health, as it addresses the pressing need for safer production practices, reduces the ecological footprint, and minimizes exposure to toxic chemicals for workers and consumers alike.

An alternative to typical single-component chromic materials might be multicomponent systems, where one chromogen can be used to generate a set of compounds with absorption depending upon the co-former incorporated in the crystal structure. The colour modifiers could be environmentally friendly molecules (here L-amino acids).

Growing interest in co-crystals and organic salts in fields such as pharmaceutical sciences[17] or optoelectronics is due to the possibility of tuning properties like stability,[18] bioavailability,[19,20]

Faculty of Chemistry, Jagiellonian University, Gronostajowa 2, 30-387 Cracow, Poland. E-mail: gryl@chemia.uj.edu.pl

† Electronic supplementary information (ESI) available: Summarized data of crystal structures included in the CSD search; crystal engineering procedures, crystal data and refinement details for studied crystalline materials; geometry of hydrogen bonds and π–π interactions observed in the studied crystals; ^{1}H NMR data for the crystallisation solutions, their mixtures and crystallised dissolved products; details of UV-Vis measurements and titration studies; details of LoD calculations; and details of topological analysis of electron density. CCDC 2008004–2008008. For ESI and crystallographic data in CIF or other electronic format see DOI: **https://doi.org/10.1039/d4tc03209h**

permeability[21] and SHG efficiency.[22–24] A comparable strategy involving cocrystallization techniques can be employed with chromic materials to fine-tune their absorption or emission properties.[25,26] In principle, if we understand the origin of colour in such a multicomponent system, we can tune the absorption at will. Using a co-crystal or an organic salt limits the usage of heavy metal ions and selection of a chromogen capable of forming vibrantly coloured products restricts the concentrations employed. Recently, we have demonstrated that designing intermolecular interactions between a chromogen and a co-former leads to distinctly coloured compounds.[27] The core component, violuric acid (VA)—an isonitroso derivative of barbituric acid (Fig. 2a)—is a colorless solid under ambient conditions. Deprotonation of VA during synthesis or cocrystallization results in the generation of intensely coloured products, with the hue attributable to n–π* transitions.[28] For instance, cocrystallization with tyramine, another colourless compound, produced two differently coloured salts: red and violet pseudopolymorphs. Additionally, we obtained a red-brown polymorph through a single crystal-to-single crystal phase transition. We have elucidated the colour phenomena in tyraminium violurates, and attributed it to a two-step process: (1) proton transfer between VA and tyramine and (2) redistribution of electron density within the oxime group of VA, influenced by intermolecular interactions.

This research[27] inspired us to explore the chromic phenomena of multicomponent materials containing VA, broadening our scope, which constitutes the focus of this study. Consequently, as co-formers for VA, we opted for representatives of amino acids (AA), namely: L-serine (L-Ser), L-tyrosine (L-Tyr), L-tryptophan (L-Trp), L-lysine (L-Lys), L-histidine (L-His), and L-arginine (L-Arg), as depicted in Fig. 1. This class of compounds carries a broad chemical and structural diversity, depending on the structure of the AA side chain. The presence of identical functional groups (carboxylate and ammonium in the zwitterionic form) in each amino acid, along with the fixed donor and acceptor sites in VA, simplifies the elucidation of the molecular recognition mechanism in the studied phases.

In this manuscript, we showcase six multicomponent crystalline phases, each comprising VA and a selected AA, namely: VASer (L-serine violuric acid water ⟨1/1/2⟩), VATyr (L-tyrosine violuric acid water ⟨1/1/3⟩), VATrp (L-tryptophan violuric acid ⟨1/1⟩), VATrp* (L-tryptophan violuric acid water ⟨1/1/1⟩) VAHis (L-histidinium violurate water ⟨2+/2−/2⟩) and VALys (L-lysinium violurate water ⟨2+/2−/2⟩). The names for the multicomponent solids were devised based on a nomenclature system proposed by two members of our team.[29] All, except VASer, exhibit absorption in the range of 428–586 nm. The origin of colour in these materials was extensively examined with the help of X-ray diffraction, UV-Vis spectroscopy and ^{1}H NMR studies of parent and product solutions. Binding constants for salts were determined through UV-Vis titration experiments. Analysis of weak interactions (hydrogen bonds, π–π interactions) was performed using theoretical calculations of non-covalent interaction (NCI) index[30] and QTAIM topological analysis of electron density in the solid state (Crystal17[31,32] and Topond[33]) to gain insight into the color phenomena of obtained crystalline materials.

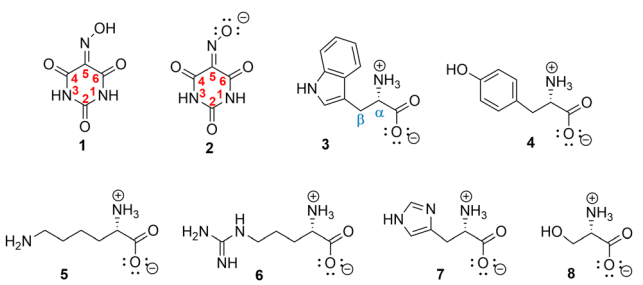

Fig. 1 violuric acid (1), violurate ion (2), L-Trp (3), L-Tyr (4), L-Lys (5), L-Arg (6), L-His (7), L-Ser (8).

Results and discussion

Crystal engineering and structure analysis

To develop multicomponent chromic materials that incorporate VA, we have strategically selected AA that exhibit diverse characteristics. L-Lysine and L-arginine were chosen as co-formers for salt formation due to their inherent basic nature. Additionally, the presence of an imidazole ring in L-His facilitates π–π stacking interactions. We also aimed to explore how weak dispersive interactions affect colour phenomena. For this purpose, we considered L-tyrosine (L-Tyr) and L-tryptophan (L-Trp), each of which has an aromatic ring in its side chain. The possibility of creating coloured crystals using VA and a co-former without aromatic rings and resistance to protonation was uncertain. L-Serine (L-Ser), a simple amino acid with a hydroxyl group in the side chain, emerged as a viable option. Its classification as a polar, uncharged amino acid, due to its hydroxyl group, contrasts with L-tryptophan's (L-Trp) non-polar characteristics. This difference could offer insights into their distinct hydrogen-bonding interactions with water molecules.

Therefore, the final selection of co-formers for cocrystallization experiments with VA includes L-Lys, L-His, L-Arg, L-Ser, L-Tyr, and L-Trp (Fig. 1). The specifics of the employed crystal engineering procedure, which includes a search for potential synthons in the CSD database, are comprehensively detailed in the ESI† (Fig. S1, S2 and Table S1).

As previously stated, a primary objective of our study was to produce either co-crystals or salts to establish whether the final colour of a product is predominantly determined by the proton transfer between an acid and a base. Typically in such a case, a pK_a rule helps to predict the possible product of cocrystallisation. This rule is based on the difference between the pK_a of a base and an acid, here $\Delta pK_a = pK_{a2}^{AA} - pK_a^A$. If ΔpK_a is less than 0, then a co-crystal formation is favoured. If the ΔpK_a is larger than 2–3 a salt formation is expected. This rule, however, does not correctly predict the formation of co-crystal or salt, if ΔpK_a is in the range of 0–2/3. The rule has been validated only for scenarios involving acid–base pairs where either a single proton is transferred, or specifically, where the transfer involves the most acidic proton of the acid to the most basic atom of the base, considering only interactions associated with the first ionization constant.[34]

Table 1 The pK_a values for VA and studied amino acids[35] where pK_{a1} is a dissociation constant of the oxime/α-carboxylic group, pK_{a2} for the α-amine group and pK_{a3} for amine groups of the amino acid side chain. In case of VA, pK_{a2} and pK_{a3} are constants for amine groups of VA ring

	VA	L-Trp	L-Tyr	L-Lys	L-Arg	L-His	L-Ser
pK_{a1}	4.35	2.38	2.24	2.15	2.03	1.70	2.13
pK_{a2}	9.64	9.34	9.04	9.16	9.00	9.09	9.05
pK_{a3}	14.2	—	10.10	10.67	12.10	6.04	—
PI	—	5.89	5.66	9.74	10.76	7.59	5.68
ΔpK_a		1.54	1.31	5.39	6.41	3.24	1.33
		VATrp Co-crystal	VATyr Co-crystal	VALys Salt	VAArg Salt	VAHis Salt	VASer Co-crystal

For the sake of comparison Table 1 presents the pK_a values for VA, L-Ser, L-Tyr, L-Trp, L-Lys, L-His and L-Arg as well as obtained values of isoelectric point (PI) for a particular amino acid. We have included the ΔpK_a values calculated as a difference between the pK_{a1} of VA and PI of the amino acid.

All the above considerations helped us to obtain four co-crystals: VASer, VATyr, VATrp, and VATrp* and two salts: VALys and VAHis. Despite multiple attempts to crystallize VAArg for X-ray diffraction analysis using various techniques, the resulting dark purple product was amorphous, not crystalline. All of the obtained phases crystallise in noncentrosymmetric space groups with amino acids as zwitterions in their L-form (crystallographic data and refinement details are given in Table S2 and asymmetric units are shown in Fig. S3, ESI†).

In the VASer co-crystal, the molecule of VA forms intermolecular interactions with four water molecules, which in turn reduces the potential for hydrogen bonding with L-Ser. Three distinct hydrogen-bond motifs between VA and L-Ser can be recognized: $R_2^2(9)$ and $R_1^2(6)$ rings, and $D_1^1(2)$ discrete motif (Fig. 2a) at the second and first graph-set level,[36] respectively. All three motifs are formed through N–H···O interactions, with nitrogen atoms from VA's NH group or AA's NH_3^+ as donors and oxygen atoms from carboxylate or carbonyl groups as acceptors. The hydroxyl group on the L-Ser's side-chain binds with two water molecules, a result of the polar O–H group's strong affinity for water. In the three remaining co-crystal structures, the arrangement of water molecules around VA varies: four water molecules interact with VA in VATyr, two water molecules associate with VA in VATrp*, and no solvent molecules are incorporated in VATrp structure.

In these three co-crystals, two specific interactions/motifs between VA and amino acid can be recognized. The first one is a hydrogen bond of the O–H···O type (marked as a pink ellipse in Fig. 2b–d) involving the O–H oxime group and the carboxylate oxygen atom of L-Tyr or L-Trp. The second motif is an $R_3^3(12)$ ring (shown in yellow in Fig. 2b–d) incorporating the first motif and additional two hydrogen bonds: N8B–H8B3···O4A^{iv} and N8B–H8B1···O91B^{iv} (in VATyr) or N11B–H11D···O4A^{iv} and N11B–H11A···O13B^{iv} (in VATrp). Moreover, in both VATyr and VATrp structures, zig-zag shaped hydrogen bonds along [100] and [010] form the $C_1^1(5)$ motif *via* N8B–H8B1···O91B^{iv} and N11B–H11A···O13B^{iv} hydrogen bonds (Fig. 2b and c), respectively. Such an architecture of hydrogen bonds leads to a parallel arrangement of phenol (L-Tyr) and indole (L-Trp) groups with VA molecules allowing π–π interactions to be present (what will be discussed later). Analysing the crystal structures of salts: VALys and VAHis, it can be seen that the number of water molecules engaged in hydrogen bonds with VA is reduced to two per anion. Water molecules function as connectors, offering steric complementarity for the densest possible packing arrangement (1.526 and 1.661 g cm^{-3} VALys and VAHis, respectively). Salt bridges between lysinium cations in VALys and histidinium ones in VAHis lead to the crystal structure built of alternate and interconnected by hydrogen bond layers of violurate anions and lysinium/histidinium cations (Fig. S4, ESI†). Detailed geometrical parameters of all hydrogen bonds can be found in Table S3 (ESI†) and hydrogen bonds around the

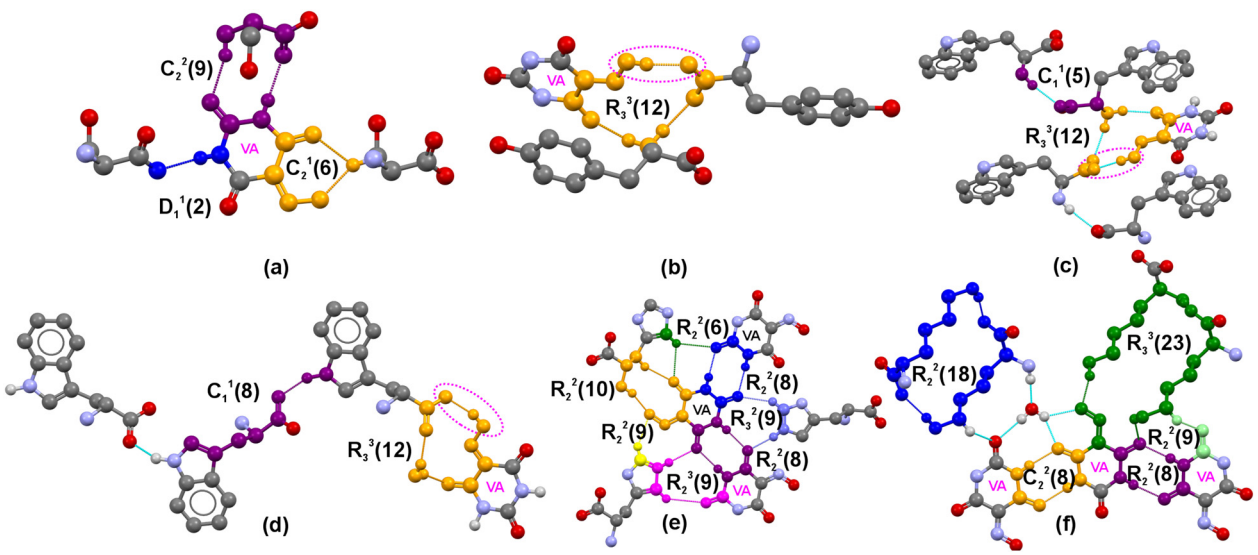

Fig. 2 Recognized synthons (shown in colour) in the (a) VASer, (b) VATyr, (c) VATrp, (d) VATrp*, (e) VAHis and (f) VALys crystal structures. Hydrogen atoms which do not participate in hydrogen bonds were omitted for clarity.

VA oxime are depicted in Fig. S5 (ESI†). As we expected from the synthon formation analysis based on the CSD search, in salt crystal structures, *i.e.* VALys and VAHis, the $R_2^2(8)$ ring motifs are observed. However, in co-crystals (VASer, VATyr and VATrp), these synthons were replaced by interactions with AA or water molecules.

Conformation and π–π interactions

Structural analysis revealed that in all co-crystals, both the ammonium group and the side chain group—hydroxyl in L-Ser, phenyl in L-Tyr, and indole in L-Trp—adopt a synclinal conformation along the C_α–C_β bond (χ_1). Torsion angles are equal to 57.77° in VASer, −65.83° in VATyr, −49.72° in VATrp and 51.28° in VATrp*. In salts, there are two independent cations of L-Lys and L-His in the asymmetric unit, namely C- and D-cations. The C-cations of L-Lys and L-His have a synclinal conformation (torsion angles χ_1 are 56.93° and −50.74°, respectively), and cations adopt antiperiplanar conformation with a torsion angle −170.30° (L-Lys) and −164.66° (L-His) – see Fig. S6 (ESI†). As was mentioned earlier, in VATyr, VATrp* and VATrp crystal structures, several π–π interactions were found. According to the literature,[37] the usual π interaction is characterized by an offset or slipped stacking arrangement. The ring normal and the vector between the ring centroids (Cg) form an angle of about 20° up to centroid–centroid distances of 3.8 Å.

The carbonyl group of VA is in the close vicinity to the phenyl ring of L-Tyr and with the 5- and 6-membered indole ring of L-Trp (Cg···Cg distances in the range of 3.24–3.56 Å). Also, the double –C=N bond of the oxime group participates in π–π interaction with L-Trp (3.40 Å). Similar interactions are observed in VAHis, where distances of Cg(C5A=N5A)···Cg(3) and Cg(C5B=N5B)···Cg(4) are 3.37 Å and 3.45 Å, respectively. Moreover, in VAHis, the O1W oxygen atom is located in close vicinity of L-His 5-membered ring with a Lp(O1W)···Cg(4) distance of 3.386 Å at an angle of 89.95°. Detailed geometrical description of all mentioned above interactions is given in Table S4 (ESI†) and the interactions are presented in Fig. S7 (ESI†). These interactions can be easily visualized using the non-covalent interaction (NCI) index.[30] NCI tool uses the reduced gradient of electron density (RDG) to highlight the low-density regime where weak and dispersive interactions can be observed. Small red or blue disks represent strong hydrogen bonds whereas broad green surfaces indicate weak non-covalent interactions. As shown in Fig. 3, the green multiform surfaces represent the π–π interactions found in VATyr, VATrp and VAHis crystal structures.

The observation of weak interactions in both dimers and larger assemblies substantiates their presence in the crystal structures. In VASer and VALys, no π–π interactions can be found.

UV-Vis and ^{1}H NMR spectroscopy, pH measurements

Absorption spectra for solution samples of VASer, VATyr, VATrp, VALys and VAHis are shown in Fig. 4a, while those for the solid state are shown in Fig. 4b. VASer crystals appeared colourless with no absorption maximum in the visible range. The slightly yellow colour of the VATyr phase corresponds to the weak absorption maximum within the range of 440–460 nm

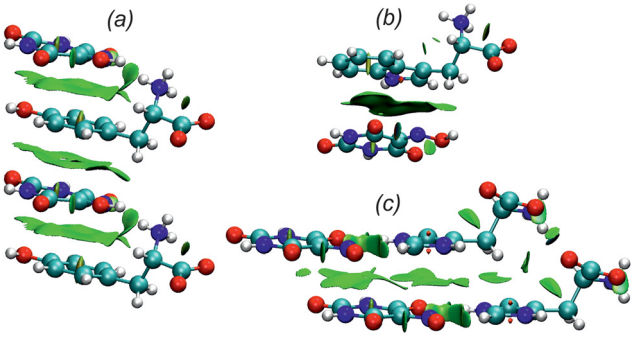

Fig. 3 NCI isosurfaces for (a) VATyr, (b) VATrp and (c) VAHis.

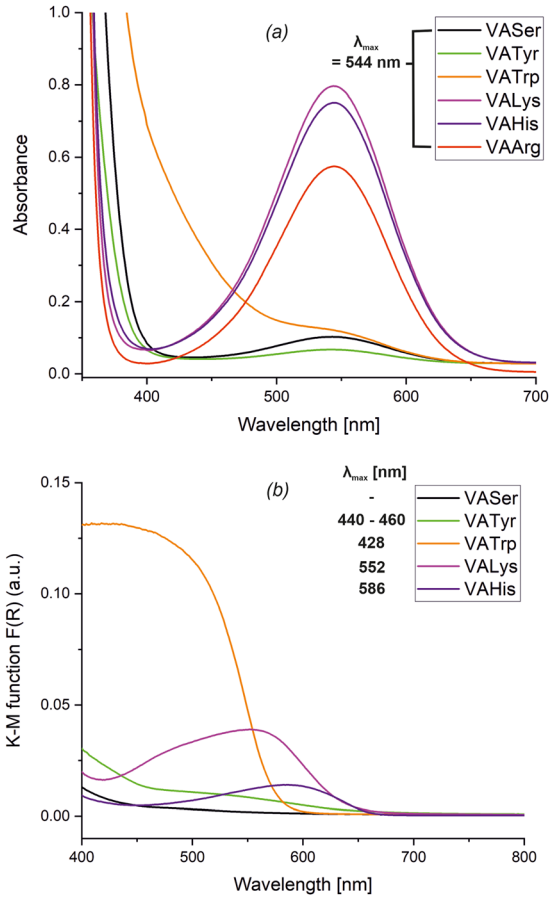

Fig. 4 The UV-Vis spectra for (a) the aqueous solutions of VA (6.72×10^{-3} M in VATyr, 1.0×10^{-2} M in VAArg and 1.42×10^{-2} M in the remaining solutions) with L-Ser (1.42×10^{-2} M), L-Tyr (6.72×10^{-3} M), L-Trp (1.42×10^{-2} M), L-Lys (1.42×10^{-2} M), L-His (1.42×10^{-2} M) and L-Arg (1.42×10^{-2} M). (b) The powdered samples of VASer, VATyr, VATrp, VALys and VAHis.

(compare Fig. S8, ESI†). Crystal phases of VATrp and VATrp* are both orange with λ_{max} at 428 nm. The absorption maxima for VALys and VAHis are at λ_{max} = 552 nm and λ_{max} = 586 nm (purple and violet colour of the crystals), respectively. In our previous study, the obtained salts of tyraminium violurates absorbed light within the range of 524–581 nm. At this stage, we can assume that the proton transfer between the oxime group of VA and AA

results in the shift of the absorption maximum towards longer wavelengths. The UV-Vis spectra for solutions of VASer, VATyr, VATrp, VALys, and VAArg are presented in Fig. 3b. The weak absorption peak at λ_{max} = 544 nm in VASer, VATyr, and VATrp solutions could be associated with the solvation effect of VA by water molecules. The strong absorption maximum at the same wavelength for VALys, VAHis and VAArg solutions can be associated with the salt formation between VA and basic AA, *i.e.* L-Arg, L-His and L-Lys. To confirm this, we have recorded the ^{1}H NMR spectra of L-His, L-Lys and L-Arg mixtures with VA (at 1 : 1 ratio) as well as the obtained products (VALys and VAHis), both in D_2O. The salt formation was monitored *via* the chemical downfield shift for the proton signals: H_a (associated with the stereogenic centre at C_α) and diasterotopic protons H_b and H_c attached to the C_β carbon atom. Formation of the NH_3^+ ammonium group at C5 of L-Lys in VALys and the L-Lys and VA mixture is manifested *via* downfield shifts and separation of signals for protons: H_a (3.24 ppm to 3.67 ppm), H_d (1.57 ppm to 1.82 ppm), H_e (1.57 ppm to 1.82 ppm), H_f (2.86 ppm to 2.94 ppm), and diasterotopic H_b and H_c (Fig. S9, ESI†). In VAHis, the protonation of the imine nitrogen atom in the L-His imidazole ring was accompanied by the shift of signals for protons of the heterocyclic system: H_d from 6.93 ppm to 7.24 ppm, and H_e from 7.63 ppm to 8.40 ppm (Fig. S10, ESI†). Protonation of L-Arg in D_2O solution after addition of VA is apparent through downfield chemical shifts and signals for H_a (3.60 ppm), H_a' (3.68 ppm), H_e, H_e' (3.14 ppm), and diasterotopic protons (Fig. S11, ESI†). We have also registered ^{1}H NMR spectra in D_2O for dissolved co-crystals of VASer and VATrp and mixtures of VA with L-Ser, L-Tyr and L-Trp (Fig. S12–S14, ESI†). The co-crystal formation was not accompanied by changes in proton chemical shifts for L-Trp, L-Tyr, and L-Ser in ^{1}H NMR data. Having established the proton transfer between VA and L-Lys, L-His, and L-Arg, along with the formation of salts in solutions, we aimed to evaluate the stability of these salts and quantify their binding constants (K). For this purpose, UV-Vis titration experiments were performed using the procedure described in the Experimental section. Fig. 5 shows the result of the spectrophotometric titrations and Fig. S15 (ESI†) presents their titration curves (absorbance as a function of components molar ratio). The Joe-Jones method[38] was used to evaluate the system stoichiometry, which was obtained from the point where the titration curve changes its slope. In each case, the stoichiometry of VA:AA was found to be 1 : 1. The binding constant was estimated using ReactLabTM EQUILIBRIA software [https://www.jplusconsulting.com] with $\log K$ = 4.955 ± 0.016 (VAArg), $\log K$ = 4.581 ± 0.006 (VALys), and $\log K$ = 3.583 ± 0.004 (VAHis). So, the obtained binding constants are as follows: $K = 9.0 \times 10^4$ M^{-1} for VAArg, $K = 3.8 \times 10^4$ M^{-1} for VALys and $K = 3.8 \times 10^3$ M^{-1} for VAHis. In comparison with other organic complexes,[39,40] these values show a moderate to high affinity of VA towards basic AA in the following order L-His < L-Lys < L-Arg. Calculated limit of detection (LoD) values are 2.54×10^{-5} M, 6.97×10^{-6} M and 8.26×10^{-6} M for VAHis, VALys and VAArg, respectively. These values show that L-Lys and L-Arg are detectable by VA at the micro level in solution samples. Details regarding LoD calculations can be found in the ESI† (Fig. S16–S18).

Hirshfeld surfaces and topological analysis of electron density

To determine the source of colour in crystalline materials, we conducted an extensive analysis of intermolecular interactions and characterized the structural features of the building blocks, as well as the crystal packing (Fig. S4, ESI†). For the comparison of intra- and intermolecular interactions of VA in co-crystals and VA anions in salts, Hirshfeld surface analysis[41] was performed. This tool is particularly useful for studying polymorphs or multicomponent crystals where one of the building blocks remains consistent.

The Hirshfeld surface of a molecule in a crystal is created by dividing the crystal space into regions where the electron density of the molecule (the promolecule), represented as a sum of spherical atoms, is greater than the electron density of the entire crystal (the procrystal). Once the Hirshfeld surface is defined, a fingerprint plot can be generated. It charts the distance from a point on the surface to the nearest external atom (d_e) against the distance to the nearest internal atom (d_i). The plot thus provides a detailed picture of how molecules in a crystal interact with their neighbors. Two-dimension fingerprint plots of VA molecule in VASer, VATyr, VATyr, VATrp and VATrp* as well as of VA anions in VALys and VAHis with percentage contribution of individual interactions are presented in Fig. 6.

We can clearly see that each image is distinct; however, there can be found some similar features such as spikes in the left and right lower parts of the graphs representing O···H and H···O interactions or wing-like motifs from C···H and H···C contacts (upper part of the drawings). The main difference between co-crystals and salts can be seen comparing O···H and H···O interactions. The amount

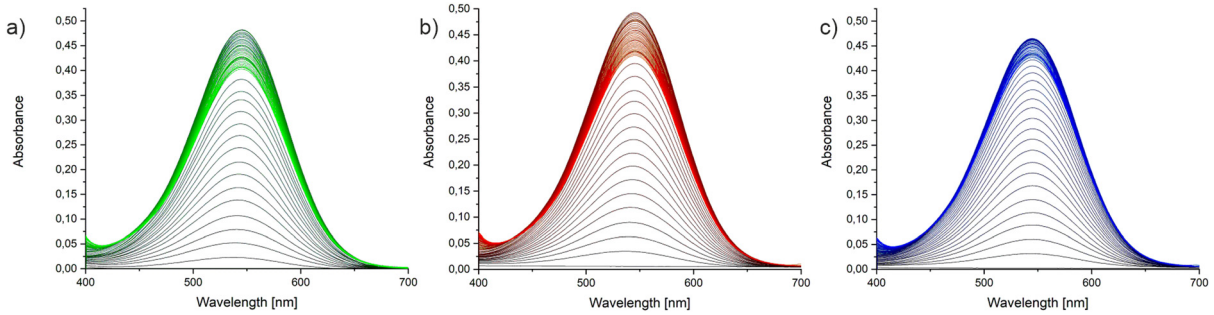

Fig. 5 Titration experiments for (a) L-Lys (b) L-Arg (c) L-His with VA.

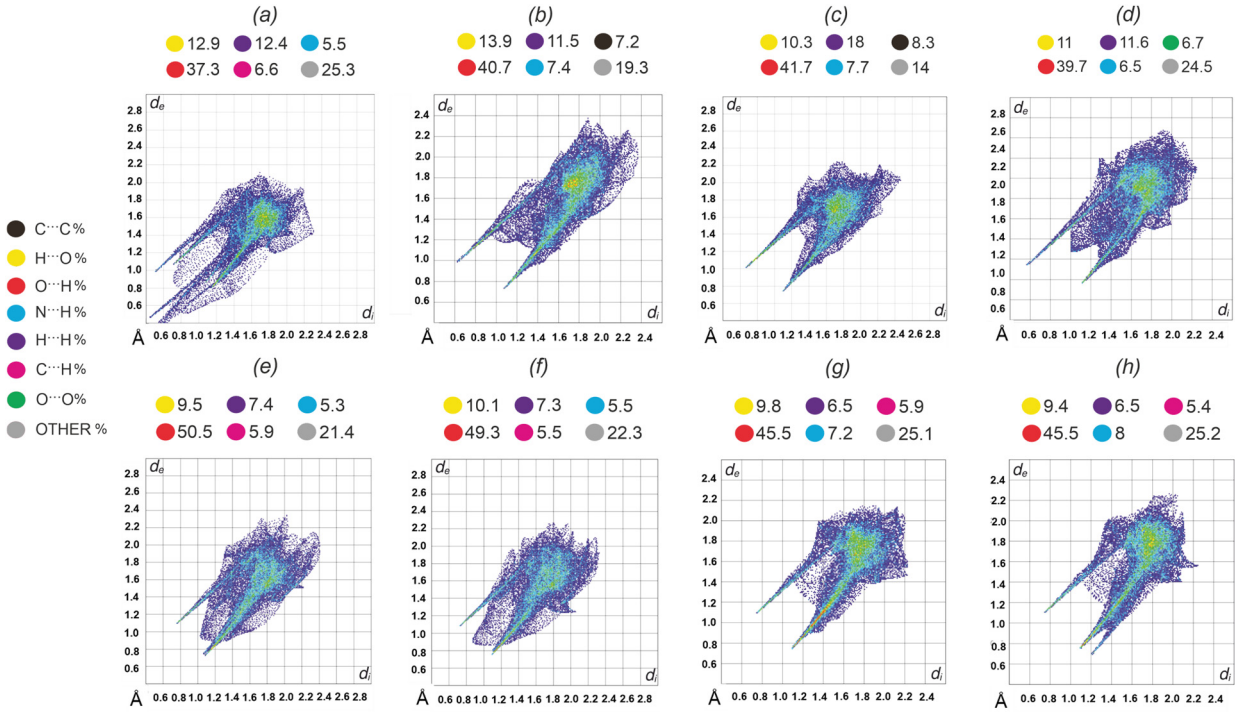

Fig. 6 Two-dimensional Fingerprint plots of VA molecules in (a) VASer, (b) VATyr, (c) VATrp*, (d) VATrp, and VA anion in (e) VALys (A anion), (f) VALys (B anion), (g) VAHis (A anion) and (h) VAHis (B anion). Coloured dots above drawings denote the percentage contribution of a particular interaction.

of O···H contacts in salts is *ca.* 8–13% larger than in co-crystals along with the slightly smaller contribution of H···O contacts. It can be also seen that in co-crystals the amount of H···H contacts (a set of dispersed points located between the spikes and in the center of the drawings) is almost as twice as that in salts. A quantitative analysis of the molecular structure and intermolecular interactions of the VA oxime group in the obtained phases was possible with QTAIM analysis.[42] The electron density derived properties at the bond critical point (BCP) for the oxime bonds: C5–N5 and N5–O5 for the studied materials and the VA monohydrate crystal structure (for comparison purposes) are presented in Table S5 (ESI†). Molecular graphs, with marked BCPs for VA molecules and ions embedded in the crystal structures, are presented in Fig. 7 and Fig. S19 (ESI†). The major differences between the salt and co-crystal structures can be seen in the bond length analysis. The N5–O5 bond becomes shorter and C5–N5 longer going from the studied co-crystals to salts. The observed increasing values of electron density $\rho(r)$ from 0.324 to 0.386 and more negative Laplacian $\nabla^2\rho(r)$ from −0.262 to −0.440, for VASer and VAHis, respectively, can be correlated with the deprotonation of VA and an accumulation of negative charge at the BCP of the N5–O5 bond. However, there are no major differences in C–N and N–O bond characteristics between two salts VALys and VAHis and this is also true for the structures of the VASer, VATyr and VATrp co-crystals. To estimate the influence of the hydrogen bonds on the electronic changes within the oxime group we have calculated the interaction energies E_O and E_N for all studied phases (E_N/E_O denotes the energy of all possible hydrogen bonds in which the N5/O5 atom of VA oxime group participates, respectively; Table S6, ESI†).[43] E_O has the largest contribution to the total energy (E_{total}) in each crystalline phase and the highest value is observed for VA and its co-crystals, whereas the interaction energy decreases gradually when going from VA to VAHis (the summarized energy components are presented in Table 2). The obtained results are in agreement with some of our previous observations made for the polymorphs of tyraminium violurates, where the smallest interaction energies E_O across polymorphs were found for violet crystals of form II (*ca.* −10.85 kcal mol^{-1}). Only small variations in energy can be found across the co-crystals: largest values of interaction energies found for VATyr and the smallest one for VATrp. Note that values presented in Table 2 were calculated per VA molecule/ion and averaged where the disordered oxime group was present. This approach allowed us to compare the VA molecule/ion in all of the examined structures. Looking at the donors and acceptors involved in the strongest hydrogen bonds (Table S4, ESI†), we can clearly see that for the co-crystals, the O5 oxygen atom plays the role of a donor whereas in

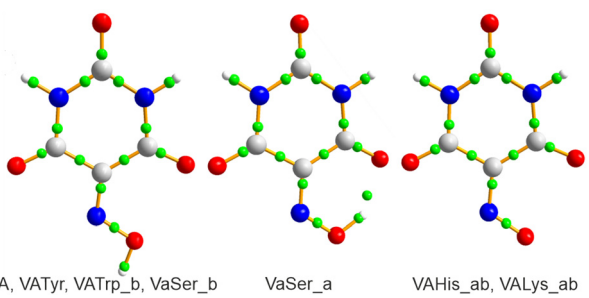

Fig. 7 Selected molecular graphs with BCPs (green) showing different conformations of VA oxime group in co-crystals, salts and VA monohydrate. The a and b denote distinct molecules/ions in the asymmetric unit.

Table 2 The sum of hydrogen bond energies involving the oxygen oxime atom (EO) and the nitrogen oxime atom (EN) of VA or its anion calculated per molecule/ion of violuric acid in each structure (optimized geometries). Energies of individual hydrogen bonds in each molecule/ion can be found in Table S6 (ESI). The procedure for estimating E_{int} can be found in ref. 43

	E_O	E_N	E_{total}
VA	−28.1		−28.1
VASer	−21.2		−21.2
VaTyr	−21.4	−5.8	−27.3
VATrp	−19.2		−19.2
VATrp*	−23.0	—	−23.0
VALys	−15.4	−4.4	−19.8
VAHis	−13.3	−2.7	−16.0

the strongest interactions in the salts, the O5 atom participates as an acceptor. Much weaker interactions (or none) are found for N5 nitrogen atoms. For the co-crystal solvates and salts, we can see a trend of decreasing interaction energies (E_{int}) with the bathochromic shift of the n–π* maximum (lower energy and longer wavelength). The case of VATrp is different as there are no solvent molecules stabilizing the structure through the hydrogen bond interactions. Instead, the hydrogen atom from the O5–H5 bond is accepted by the carboxylic oxygen atom of L-Trp. For comparison purposes, we have added a VATrp* structure which is a salt solvate (pseudopolymorph of anhydrous VATrp). In fact, we have already shown that there are no obvious changes in the colour of VATrp and VaTrp* as a result of the presence or absence of water molecules. This is the only case where we were able to obtain a crystal structure containing VA and amino acids without water molecules, although the crystals were of inferior quality.

Conclusions

We have designed, obtained and thoroughly analyzed six new crystal phases containing violuric acid (VA) and L-amino acids with diverse optical properties. Our research offers a novel perspective by demonstrating the crucial role of hydrogen bonding involving the oxime group on the absorption properties of a series of compounds. We confirmed that the intense coloration observed in some VA-based materials is linked to salt formation and the presence of VA in an anionic state. In particular, the L-amino acids with PI $>$ 7 were found to form salts with VA whereas the ones with PI $<$ 7 formed co-crystals (see Table 1). Additionally, our research resulted in the identification of various recurring synthons related to the presence of VA in both its neutral and deprotonated forms. In particular, we observed significant variations in the strength of interactions involving VA's oxime group across both salts and co-crystals. This observation supports the hypothesis that shifts in the absorption band within the visible spectrum are associated with weak interactions in these systems. Initially, one might assume that the coloration of these materials is due to π–π interactions. However, our findings reveal no direct correlation between the strength of these interactions and the position of the absorption band responsible for the colour. For instance, the intensely colored salts VALys and VAHis, with similar absorption bands (λ_{max} = 552 nm and λ_{max} = 586 nm, respectively), are different in this manner. In VALys, there are no π–π interactions, whereas in VAHis, we can find three with moderate strengths. VaSer crystals appear colourless with no absorption maximum in the visible range and no π···π interactions. Conversely, VATrp crystals, displaying a pale yellow hue (440–460 nm), exhibit the shortest Cg···Cg distances (3.24 Å) among the studied materials (see Table S4, ESI†). When examining hydrogen bonding, a different scenario emerges. We hypothesize that stronger interactions involving VA's oxime group shift the n–π* band towards the higher-energy end of the UV-Vis spectrum. This conclusion aligns with our previous research on tyraminium violurates. To confirm this hypothesis, we performed model TDDFT calculations using two clusters (Fig. S20, ESI†) constructed from the VAHis crystal structure. We selected the first cluster comprised of one VA anion, one L-His anion, and one water molecule. In this model, after optimizing the cluster, there is only one hydrogen bond, (H_2O)H···O(oxime), with an H···A distance of 1.804 Å. Additionally, we constructed a second cluster by modifying the first one, removing the water molecule. This time, after optimization, there is only one hydrogen bond, (NH_2)H···O(oxime), with an H···A distance of 2.109 Å. The subsequent TDDFT calculations (results summarized in Table S7, ESI†), indicate that changing the environment around the oxime group affects the shift of the absorption maximum towards shorter wavelengths, consistent with the strengthening of interactions involving the oxime oxygen atom. The two formed clusters demonstrate that the shift in absorption maximum correlates with the presence and nature of hydrogen bonds involving the oxime group. However, this hypothesis needs to be experimentally verified by exploring and studying the absorption properties of a single chromogen (violuric acid) with an expanded array of co-formers. This would help to assess the feasibility of designing multicomponent materials with customized chromic effects. Nonetheless, this study highlights the adaptability of VA as a versatile chromogen for designing and producing a variety of coloured materials, demonstrating its potential in material science.

Experimental

Cocrystallisation

L-Serine violuric acid water ⟨1/1/2⟩ (VASer). Equimolar amounts of VA and L-Ser were dissolved in water and mixed. The vial with crystallization solution was left for slow evaporation under ambient conditions. After a few days, colourless plate-like crystals appeared in the vial.

L-Tyrosine violuric acid water ⟨1/1/3⟩ (VATyr). Equimolar amounts of VA and L-Tyr were dissolved in acetonitrile and water, respectively. The aqueous solution of L-Tyr was heated up to *ca.* 50 °C. A mixture of VA and L-Tyr was left for slow evaporation under ambient conditions. After a week, pale yellow needle-like crystals appeared in the flask.

L-Tryptophan violuric acid ⟨1/1⟩(VATrp). Equimolar amounts of VA and L-Trp were dissolved in acetonitrile and water, respectively. The aqueous solution of L-Trp was heated up to *ca.* 80 °C. A mixture of VA and L-Trp was left for slow

evaporation under ambient conditions. After a few days, orange plate-like crystals appeared in the flask.

L-Tryptophan violuric acid water ⟨1/1/1⟩(VATrp*). Equimolar amounts of VA and L-Trp were both dissolved in water. The aqueous solution of L-Trp was heated up to *ca.* 80 °C. A mixture of VA and L-Trp was left for slow evaporation under ambient conditions. After a few days, orange very fine crystals appeared in the flask.

L-Histidinium violurate water ⟨2+/2−/2⟩(VAHis). Equimolar amounts of VA and L-His were both dissolved in water. A mixture of VA and L-His was left for slow evaporation under ambient conditions. After a few days, small violet crystals appeared in the vial.

L-Lysinium violurate water ⟨2+/2−/2⟩(VALys). Amounts of VA and L-Lys in the 2 : 1 molar ratio were dissolved in water. A mixture of VA and L-Lys was left for slow evaporation under ambient conditions. After a few days, purple needle-like crystals appeared in the vial.

Data collection and crystal structure refinement

Crystal structures of all obtained materials were determined using single crystal X-ray diffraction studies. SIR92[44] was used to solve the structure of VASer and SHELXT[45] for the remaining phases. The refinement procedure based on the F^2 least-squares method was performed using the SHELXL2018 program.[46] Aromatic and aliphatic hydrogen atoms were calculated at idealized positions and refined using a riding model. The remaining hydrogen atoms were found from different Fourier maps and refined freely with U_{iso} = 1.2 U_{iso}(parent atom). Crystal data, details of data collection, and structure refinement for all crystal structures are given in Table S2 (ESI†). In some of the crystal structures, the oxime group is disordered. In VASer, site occupancy factors for N5A–O5A and N5A1–O5A1 pairs are 0.58 : 0.42; in VATrp N5A–O5A and N5A1–O5A1, atom pairs are disordered over two positions in ratio 0.67 : 0.33; in VALys oxime O5A : O5A′ atoms are in ratio 0.87 : 0.13 and disordered CH2 groups in L-lysine are in ratio 0.12 : 0.88 (C2′/C3′ : C2/C3). Additionally, in VAHis, O21W–H211 and O22W–H221 pairs of atoms in one of the water molecules are disordered in ratio 0.61 : 0.39, respectively.

Theoretical calculations

Non-covalent interaction (NCI) index calculations were performed using NCIPLOT software.[30] The input wavefunctions were calculated with the M052X/6-311+G(2df,2p) level of theory using GAUSSIAN16 software (Revision C.01).[47]

Test TDDFT calculations were carried out in Gaussian16 using B3LYP/6-31G(2d,2p).

The input wavefunctions for the theoretical electron density calculations were determined using the Crystal17[31,32] software at the PBEsol0/POB-TZVP level of theory. The geometry of the molecules and ions was optimized with fixed lattice parameters. Topond[33] was used for the topological analysis of electron density.

The M052X developed by Zhao and Truhlar[48–51] has been shown to correctly describe noncovalent interactions.[52] This functional was used for the NCI calculations that allowed a reliable description of weak, dispersive interactions.[53]

On the other hand, periodic calculations were performed with PBEsol0 functional which is a PBE0 revised specifically for solids.[54,55] Both PBEsol and PBEsol0 were proven to correctly describe unit cell parameters as well as intermolecular interactions in solids.[56,57]

^{1}H NMR spectroscopy

The ^{1}H NMR spectra for 5 mg of L-Ser, L-Tyr, L-Trp, L-Lys, L-His and L-Arg, a mixture of VA and AA in 1 : 1 ratio (5 mg of VA, 3 mg of L-Ser, 5 mg of L-Tyr, 6 mg of L-Trp, 4 mg of L-His, 4 mg of L-Lys and 5 mg of L-Arg), and isolated 5 mg of VAHis and VALys salts and VATrp and VASer co-crystals in 1 mL D2O were recorded using a Bruker Avance III 600 at 300 K. The ^{1}H NMR spectra were referenced internally to the residual proton resonance in D_2O.

UV-Vis spectroscopy

All UV-Vis experiments were carried out using a PerkinElmer LAMBDA 365 Spectrophotometer at room temperature. Grinded solid-state samples of VASer, VATyr, VATrp, VALys and VAHis were mixed with barium sulphate, and spectra were registered using the 50 mm transmission/reflectance sphere whereas UV-Vis spectra for solutions were recorded in 1 cm quartz cells. The titration experiment for VAHis, VALys, and VAArg salts was performed as follows: the stock 2 mL 0.01 M solution of a particular amino acid (L-His, L-Lys, L-Arg) was titrated with 20 μL of VA solution (0.05 M) and the spectrum was recorded after each addition. The total number of added equivalents for each salt was 50.

Author contributions

This publication was written with contributions from all authors.

Data availability

The data supporting this article have been included as part of the ESI.† Crystallographic data for all the mentioned compounds has been deposited at the CCDC under CCDC deposition numbers 2008004–2008008.

Conflicts of interest

There are no conflicts to declare.

Acknowledgements

This work was carried out with equipment purchased thanks to the financial support of the European Regional Development Fund in the framework of the Polish Innovation Economy Operational Program (contract No. POIG.02.01.00–12-023/08) and the Ministry of Science and Higher Education, Warsaw, Poland (grant number 6903/IA/SP/2018). This research was

supported by the National Science Centre, grant number 2018/30/E/ST5/00638. We gratefully acknowledge Polish high-performance computing infrastructure PLGrid (HPC Center: ACK Cyfronet AGH) for providing computer facilities and support within computational grant no. PLG/2023/016132.

Notes and references

1 A. Buryak and K. Severin, *J. Am. Chem. Soc.*, 2005, **127**, 3700–3701.
2 F. Sancenón, A. B. Descalzo, R. Martínez-Máñez, M. A. Miranda and J. Soto, *Angew. Chem., Int. Ed.*, 2001, **40**, 2640–2643.
3 T. Minami, N. A. Esipenko, B. Zhang, L. Isaacs and P. Anzenbacher, *Chem. Commun.*, 2014, **50**, 61–63.
4 H. Y. Fu, X. J. Liu and M. Xia, *RSC Adv.*, 2017, **7**, 50720–50728.
5 Z. Zhao, H. Nie, C. Ge, Y. Cai, Y. Xiong, J. Qi, W. Wu, R. T. K. Kwok, X. Gao, A. Qin, J. W. Y. Lam and B. Z. Tang, *Adv. Sci.*, 2017, **4**, 1–8.
6 M. De Bastiani, M. I. Saidaminov, I. Dursun, L. Sinatra, W. Peng, U. Buttner, O. F. Mohammed and O. M. Bakr, *Chem. Mater.*, 2017, **29**, 3367–3370.
7 P. Bamfield and M. Hutchings, *Chromic Phenomena*, RSC, 3rd edn, 2018.
8 N. Bar and P. Chowdhury, *ACS Appl. Electron. Mater.*, 2022, **4**, 3749–3771.
9 M. Martínez-Junquera, E. Lalinde and M. T. Moreno, *Inorg. Chem.*, 2023, **62**, 11849–11868.
10 F. Robert, P. L. Jacquemin, B. Tinant and Y. Garcia, *CrystEngComm*, 2012, **14**, 4396–4406.
11 D. A. Safin, M. Bolte and Y. Garcia, *CrystEngComm*, 2014, **16**, 5524–5526.
12 M. Morimoto, R. Kashihara, K. Mutoh, Y. Kobayashi, J. Abe, H. Sotome, S. Ito, H. Miyasaka and M. Irie, *CrystEngComm*, 2016, **18**, 7241–7248.
13 R. Hagihara, T. Umeno, S. Ueki, D. Yoshihara, Y. Fuchi, K. Usui, M. Sakuma, K. Ichi Yamada and S. Karasawa, *Chem. – Eur. J.*, 2021, **27**, 3039–3046.
14 R. Tan, Q. Lin, Y. Wen, S. Xiao, S. Wang, R. Zhang and T. Yi, *CrystEngComm*, 2015, **17**, 6674–6680.
15 K. Golka, S. Kopps and Z. W. Myslak, *Toxicol. Lett.*, 2004, **151**, 203–210.
16 B. Lellis, C. Z. Fávaro-Polonio, J. A. Pamphile and J. C. Polonio, *Biotechnol. Res. Innov.*, 2019, **3**, 275–290.
17 K. Shiraki, N. Takata, R. Takano, Y. Hayashi and K. Terada, *Pharm. Res.*, 2008, **25**, 2581–2592.
18 A. V. Trask, W. D. S. Motherwell and W. Jones, *Int. J. Pharm.*, 2006, **320**, 114–123.
19 J. R. Wang, X. Yu, C. Zhou, Y. Lin, C. Chen, G. Pan and X. Mei, *Bioorganic Med. Chem. Lett.*, 2015, **25**, 1036–1039.
20 S. Golob, M. Perry, M. Lusi, M. R. Chierotti, I. Grabnar, L. Lassiani, D. Voinovich and M. J. Zaworotko, *J. Pharm. Sci.*, 2016, **105**, 3626–3633.
21 X. L. Dai, J. Yao, C. Wu, J. H. Deng, Y. H. Mo, T. B. Lu and J. M. Chen, *Cryst. Growth Des.*, 2020, **20**, 5160–5168.
22 J. Wojnarska, M. Gryl, T. Seidler, A. Rydz, M. Oszajca, K. M. Stadnicka, M. Marzec, I. Matulková, I. Němec and P. Němec, *Cryst. Growth Des.*, 2019, **19**, 6831–6836.
23 M. Gryl, T. Seidler, J. Wojnarska, K. Stadnicka, I. Matulková, I. Němec and P. Němec, *Chem. – Eur. J.*, 2018, **24**, 8727–8731.
24 E. D. D'Silva, G. K. Podagatlapalli, S. V. Rao, D. N. Rao and S. M. Dharmaprakash, *Cryst. Growth Des.*, 2011, **11**, 5362–5369.
25 B. Lu, Y. Zhang, X. Yang, K. Wang, B. Zou and D. Yan, *J. Mater. Chem. C*, 2018, **6**, 9660–9666.
26 L. Sun, W. Zhu, X. Zhang, L. Li, H. Dong and W. Hu, *J. Am. Chem. Soc.*, 2021, **143**, 19243–19256.
27 M. Gryl, A. Rydz, J. Wojnarska, A. Krawczuk, M. Kozieł, T. Seidler, K. Ostrowska, M. Marzec and K. M. Stadnicka, *IUCrJ*, 2019, **6**, 226–237.
28 R. M. Awadallah, A. A. M. Belal, R. M. Issa and R. D. Peacock, *Spectrochim. Acta*, 1994, **47A**, 1541–1546.
29 M. Gryl, M. Kozieł and K. M. Stadnicka, *Acta Crystallogr., Sect. B: Struct. Sci., Cryst. Eng. Mater.*, 2019, **75**, 53–58.
30 J. Contreras-García, E. R. Johnson, S. Keinan, R. Chaudret, J. P. Piquemal, D. N. Beratan and W. Yang, *J. Chem. Theory Comput.*, 2011, **7**, 625–632.
31 R. Dovesi, V. R. Saunders, C. Roetti, R. Orlando, C. M. Zicovich-Wilson, F. Pascale, B. Civalleri, K. Doll, N. M. Harrison, I. J. Bush, P. D'Arco, M. Llunel, M. Causà, Y. Noël, L. Maschio, A. Erba, M. Rérat and S. Casassa, *CRYSTAL17 User's Man.*, 2018, 211.
32 R. Dovesi, A. Erba, R. Orlando, C. M. Zicovich-Wilson, B. Civalleri, L. Maschio, M. Rérat, S. Casassa, J. Baima, S. Salustro and B. Kirtman, *Wiley Interdiscip. Rev. Comput. Mol. Sci.*, 2018, **8**, 1–36.
33 C. Gatti and S. Casassa, *TOPOND14 User's Manual, CNR-ISTM*, Milano, Italy, 2013.
34 A. J. Cruz-Cabeza, *CrystEngComm*, 2012, **14**, 6362–6365.
35 D. R. Lide, *Handbook of Chemistry and Physics*, CRC Press, 85th edn, 2004–2005.
36 M. C. Etter, J. C. MacDonald and J. Bernstein, *Acta Crystallogr., Sect. B*, 1990, **46**, 256–262.
37 C. Janiak, *J. Chem. Soc. Dalton Trans.*, 2000, 3885–3896.
38 J. M. Bosque-Sendra, E. Almansa-Lopez, A. M. Garcia-Campana and L. Cuadros-Rodriguez, *Anal. Sci.*, 2003, **19**, 1431–1439.
39 A. A. Altaf, U. Hashmat, M. Yousaf, B. Lal, S. Ullah, A. A. Holder and A. Badshah, *R. Soc. Open Sci.*, 2016, **3**(11), 1–12, DOI: 10.1098/rsos.160351.
40 R. Ghosh and B. Singh, *Indian J. Chem., Sect. A: Inorg., Phys., Theor. Anal.*, 1980, **19**, 1102–1105.
41 J. J. McKinnon, D. Jayatilaka and M. Spackman, *Chem. Commun.*, 2007, 3814.
42 R. F. W. Bader, *Preface*, Oxford Clarendon Press, vol. 22, 2003.
43 E. Espinosa, E. Molins and C. Lecomte, *Chem. Phys. Lett.*, 1998, **285**, 170–173.
44 A. Altomare, G. Cascarano, C. Giacovazzo, A. Guagliardi, M. C. Burla, G. Polidori and M. Camalli, *J. Appl. Crystallogr.*, 1994, **27**, 435.
45 G. M. Sheldrick, *Acta Crystallogr., Sect. A: Found. Crystallogr.*, 2015, **71**, 3–8.
46 G. M. Sheldrick, *Acta Crystallogr., Sect. C: Struct, Chem.*, 2015, **71**, 3–8.

47 M. J. Frisch, G. W. Trucks, H. B. Schlegel, G. E. Scuseria, M. A. Robb, J. R. Cheeseman, G. Scalmani, V. Barone, G. A. Petersson, H. Nakatsuji, X. Li, M. Caricato, A. V. Marenich, J. Bloino, B. G. Janesko, R. Gomperts, B. Mennucci, H. P. Hratchian, J. V. Ortiz, A. F. Izmaylov, J. L. Sonnenberg, D. Williams-Young, F. Ding, F. Lipparini, F. Egidi, J. Goings, B. Peng, A. Petrone, T. Henderson, D. Ranasinghe, V. G. Zakrzewski, J. Gao, N. Rega, G. Zheng, W. Liang, M. Hada, M. Ehara, K. Toyota, R. Fukuda, J. Hasegawa, M. Ishida, T. Nakajima, Y. Honda, O. Kitao, H. Nakai, T. Vreven, K. Throssell, J. A. Montgomery Jr., J. E. Peralta, F. Ogliaro, M. J. Bearpark, J. J. Heyd, E. N. Brothers, K. N. Kudin, V. N. Staroverov, T. A. Keith, R. Kobayashi, J. Normand, K. Raghavachari, A. P. Rendell, J. C. Burant, S. S. Iyengar, J. Tomasi, M. Cossi, J. M. Millam, M. Klene, C. Adamo, R. Cammi, J. W. Ochterski, R. L. Martin, K. Morokuma, O. Farkas, J. B. Foresman and D. J. Fox, *Gaussian 16, Revision C.01*, Gaussian, Inc., Wallingford CT, 2016.
48 Y. Zhao, N. E. Schultz and D. G. J. Truhlar, *Chem. Phys.*, 2005, **123**, 161103.
49 Y. Zhao, N. E. Schultz and D. G. J. Truhlar, *Chem. Theory Comput.*, 2006, **2**, 364–382.
50 Y. Zhao and D. G. J. Truhlar, *Chem. Phys.*, 2006, **125**, 194101.
51 Y. Zhao and D. G. Truhlar, *Theor. Chem. Acc.*, 2008, **120**, 215–241.
52 E. G. Hohenstein, S. T. Chill and C. D. Sherrill, *J. Chem. Theory Comput.*, 2008, **4**(12), 1996–2000.
53 Y. Zhao and D. G. Truhlar, *J. Chem. Theory Comput.*, 2007, **3**(1), 289–300.
54 J. P. Perdew, A. Ruzsinszky, G. I. Csonka, O. A. Vydrov, E. Scuseria, L. A. Constantin, X. Zhou and K. Burke, *Phys. Rev. Lett.*, 2008, **100**(13), 136406.
55 C. Adamo and V. Barone, *J. Chem. Phys.*, 1999, **110**(13), 6158–6170.
56 A. V. Terentjev, L. A. Constantin and J. M. Pitarke, *Phys. Rev. B*, 2018, **98**, 214108.
57 J. Quertinmont, A. Carletta, N. A. Tumanov, T. Leyssens, J. Wouters and B. Champagne, *J. Phys. Chem. C*, 2017, **121**, 6898–6908.